Type of contribution:
Editorial
▶ Research Paper
Case Study
Review Paper
Scientific Data
Report of Tech. Application

e-issn. 2798-5245

Mechanical Engineering for Society and Industry
Vol. 4, No. 1 (2024) pp 5-16
https://doi.org/10.31603/mesi.10492

Optimal design of stator slot with semi-closed type to maximize magnetic flux connection and reduce iron leakage in high-speed spindle drives

Wawan Purwanto[1]*, Firoj Mulani[2], Krismadinata[3], Hasan Maksum[1], Ahmad Arif[1], Dwi Sudarno Putra[1], Kathleen E. Parigalan[4]

[1] Department of Automotive Engineering, Universitas Negeri Padang, Padang 25131, **Indonesia**
[2] Department of Electrical Engineering, Southern Taiwan University of Science and Technology, Tainan 710, **Taiwan**
[3] Department of Electrical Engineering, Universitas Negeri Padang, Padang 25131, **Indonesia**
[4] Department of Electro-Mechanical Technology, University of Science and Technology of Southern Philippines, 9000, **Philippines**
✉ wawan5527@ft.unp.ac.id

This article contributes to:

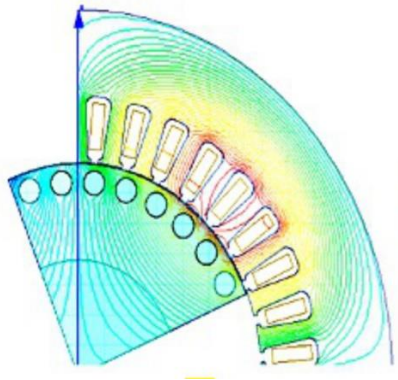

Highlights:

- A new method for optimizing stator slot design through a combined response surface approach and finite element analysis is used in this study.
- Slot geometry, coil configuration and wire size are optimized to achieve larger flux junctions and lower iron leakage.
- Experimental validation shows substantial improvement in flux connections and reduction in iron leakage.

Abstract

A novel approach was devised to optimize the stator slot semi-closed type in order improve the magnetic flux connection and minimize iron leakage in high-speed spindle drives. The concept was executed through a combination of response surface approach including the technique of finite element analysis. The primary objective of this investigation would be to provide an engineering approach which improves the functionality of stator criteria, including the stator slot geometry, coil turn per slot, and wire size. The purpose is to achieve higher flux connection and minimize iron leakage. This study presents an enhanced analytical approach that incorporates the analysis of stator flux connection, finite element calculation of flux connection, and iron leakage analysis of stator variables. The results are analyzed through the utilization of finite element computation, and their accuracy is verified through experimental measurements. The findings suggest the ideal design yields increased magnetic flux connection and reduced iron leakage in comparison to the industrial layout. The precision provided by the suggested model is confirmed through the comparison of the simulation and experimental information. In general, the percentage of errors is estimated to be around 7%.

Keywords: Finite element method; Iron leakage; Magnetic flux connection; Response surface approach; Stator variable

Article info
Submitted: 2023-11-05
Revised: 2023-12-24
Accepted: 2023-12-27

Publisher
Universitas Muhammadiyah Magelang

1. Introduction

High-speed spindle motors are extensively utilized in both traditional and contemporary manufacturing equipment across many industrial sectors. Spindle devices are utilized due to their notable toughness, uncomplicated construction, and cost-effectiveness. These tools demonstrate outstanding reliability by achieving excellent efficiency and output while minimizing wasted energy. The operational efficiency of a spindle machine is significantly affected by magnetic flux connection and iron leakage. It is imperative for manufacturers to

possess a comprehensive understanding of the impact of stator variables on electromagnetic and magnetic characteristics to successfully manage flux connection and iron waste. Hence, to achieve a spindle motor with superior efficiency, it is imperative to accurately calculate the stator variables during the optimization and fabrication stages. This is crucial for minimizing leakage and maximizing flux connection.

Various methods of manufacture, including drilling, machining, clenching, and the welding process, possess the potential to adversely affect the magnetism of electrical assemblies. Consequently, those procedures could result in a boost in stator permeability reactance and elimination of iron [1]. The utilization of sewing or boring instruments in processing steps has a direct impact on the exterior of the stator groove [2], hence influencing multiple variables such as the flux of magnetism factor, stator back iron grief, and stator yoke mass [3]. The technique of manual sewing has been seen to result in the degradation of the iron plate near the sliced surface [4]. Variations in the dimensions of stator grooves result in disparities in magnetism exhaustion, slot permeability reaction, and copper leakage. The parameters that influence the flux connection, stator groove flux density, and flux pulsating elimination include the total number of coils, thickness of the slot crossing, the dimension of the stator core, which are the size of the stator groove [5]. The stator grooves have a significant impact on various aspects of thermal energy preservation, such as stator leaking reaction, electromagnetic flux connection, and extra energy loss [6]. The development of a high-speed spindle drive can be achieved by employing several techniques such as expert stationary spindle architecture [7], the Taguchi approach, and finite element method (FEM) as well as response surface methodology (RSM) and FEM [8]. The achievement of the RSM was made simpler through the utilization of the experimental layout strategy in conjunction with the Finite Element approach (FEM), hence enabling the efficient analysis of complicated challenges [9].

In accordance with previous investigations, it was determined to optimize the stator variables employing an RSM and FEM, to increase magnetic connection and reduce iron leakage triggered by fluctuations in portions of the stator variables in a high-speed spindle machine. The stator variable approach described below was designed specifically for machining operations characterized by rotational rates spanning from 3000 to 21000 revolutions per minute (rpm). A design of experiment (DOE) was undertaken using the central composite design (CCD) strategy for the purpose of constructing a second-order representation of stator and iron leaking concentration. In conjunction with flux linkages finite element analysis (FEM), this mathematical framework was employed to examine the impact of stator characteristics on many aspects, including stator leaking, magnetic flow connection, iron reduction, as well as torque and efficiency of the spindle drive. In conclusion, an investigation was conducted on the magnetic flux connection and iron damage. To validate the computational findings, a prototype device was constructed and conducted to testing at rotational speeds of 3000, 12000, and 21000 rpm, using the IEEE standard 112-method B test [10].

2. Magnetic Flux and Iron leakage investigation

To achieve a successful design technique that meets the required specifications, many analyses are being conducted. These include an examination of the stator flux connection, a finite element method (FEM) study of the flux characteristics, and an assessment of iron leakage while considering variations in the stator variables. The present investigations have been undertaken to evaluate the specifications of the design. Through the utilization of this study, it becomes possible to identify the essential design variables by means of statistical assessment, ultimately leading to the attainment of the desired design goals.

2.1. The Examination of Stator Flux Connection by Considering Stator Geometry

In order to create flux connection, it is necessary for the flux created by the stator to traverse the airgap and encompass the rotor conductor, also known as the rotor bar. Nevertheless, it should be noted that not all lines of flux establish a connection between the coil of the stator and rotor. There is a presence of tiny leakage of flux at many locations, including slots, airgaps (referred to as weaving leaking), and end twists. The phenomenon of slot leaking flux occurs at different elevations within the groove. The generation of each flux line is facilitated by the currents that

build up in the stator circuit. The expression of the total flux connection is determined by the combined stator and rotor slot geometry, as stated in Eq. (1).

$$\psi = \mu_0 \left(\frac{hs_0}{bs_0} + \frac{2hs_1}{bs_1 + bs_2} + \frac{hs}{bs_2} + \frac{3hs_1}{3bs_2} \right) L_i I_s \tag{1}$$

or

$$\psi = \mu_0 L_i I_s S_0 \tag{2}$$

where the groove permeance ratio symbolized by S0, which can be employed to design specific slot designs, is located at a particular location. Moreover, assuming that the total coil is denoted as *Ns*, it follows that the total of slots per phase can be expressed as N_1/q. Additionally, the flux linkage of the phase winding can be determined using Eq. (3).

$$\psi_{ps} = \mu_0 L_i I_s S_0 \left(\frac{N_1}{q} \right) \left(\frac{2qN_s}{N_1} \right)^2 \tag{3}$$

The stator leakage reactance (Ls) per phase is declared by Eq. (4).

$$L_s = \frac{\psi_{ps}}{I_s} = \mu_0 L_i S_0 \left(\frac{N_1}{q} \right) \left(\frac{2qN_s}{N_1} \right)^2 \tag{4}$$

where the variable L_i represents the overall length of the stator, specifically referring to the length of the stator circuits that are inserted into the iron. The stator phase electrical current (*Is*) encompasses a strong correlation with the coil, wire diameter, and stator resistance. Equation (4) demonstrates the ideal stator phase electrical current, which results in reduced stator leaking and increased flux connection of every phase coil. The flow of magnetic connection at the recommended speed could be determined using other equivalent circuit techniques as presented in Eq. (5), which use the stator phase current, stator resistance (R_2), and stator linking reactance.

$$\psi_s = \frac{\sqrt{2}|V_{ph} - I_s R_2}{\omega_m} \tag{5}$$

2.2. Flux Connection Stator to Rotor Winding using FEM Technique

The determination of the total flux per pole is based on the analysis of the flux circulation, whose is primarily influenced by various factors including the physical dimensions of the electric motor, the configuration of the winding inside the stator, the distance of the airgap, the permeation rate of the stator core materials, and the force of electricity. The flux concentrations within the coil of the stator are affected by the fluctuating reluctances present in both the stator and rotor teeth, along with the level of saturation of the core itself [11]. While a three-phase power balanced, sinusoidal electricity is given to the spindle drive, the electricity that results could differ from perfectly harmonic behavior due to the presence of irregular characteristics of the material. In the case of the current assessment being conducted, the coils A, B, and C are subjected to equal pulsating magnetically attracting currents. The determination of the electric field within the range of vector possible A is easily achieved by employing the Eq. (6), which corresponds to the 2D Maxwell model for magnetic potentially transitory finite element method (FEM) assessment (Eq. 7), and further by utilizing the Euler equation of the nonlinear energy function (Eq. 8) for flux connection FEM calculations [12].

$$A = \frac{(\mu_0 \div 4\pi)\varphi d L_i}{r} \tag{6}$$

$$\frac{\partial}{\partial x}\left(\frac{1}{\mu_0} \frac{\partial A}{\partial x} \right) + \frac{\partial}{\partial y}\left(\frac{1}{\mu_0} \frac{\partial A}{\partial y} \right) - \sigma \frac{dA}{dt} + J = 0 \tag{7}$$

$$F = \iint_R \left(\int_0^B vb \, db \right) dx \, dy - \iint_R JA \, dx \, dy \tag{8}$$

In the scenario at hand, *A* represents the magnetization possibility, μ_0 denotes the permeable nature of the magnetized substance, *r* signifies the circumference of a uniform conductor, *J* represents the electrical current concentration at a particular point in time *t*, *b* denotes the field of magnetic attraction, and σ represents the corresponding conduction of the rotor bar. The expression of the flux connected by a coil can be formulated in relation to the flux concentration in the B and the contained region of the stator winding's circumference. Thus, flux connection in the stator to the rotor configuration can be express by Eq. (9).

$$\emptyset = \int B \, dS \tag{9}$$

Then the flux magnetizing can be computed as

$$\emptyset = \int (\nabla \mathrm{A}) \, dS \tag{10}$$

If the shape of the vector representing the possible magnetic flux on the correct side of the conducting turn is denoted as A_{RH}, and the vector representing the prospective magnetic energy on the left side of the coil turn is denoted as A_{LH}, the total flux linkage can be estimated by Eq. (11).

$$\psi = N_0 \emptyset = N_s L_i (A_{RH} - A_{LH}) \tag{11}$$

2.3. Iron Leakage Analysis by Considering Stator Slot with Semi-closed Type Changes

The primary source of stray losses in a fast spindle drive is the iron leakage caused by fundamental iron loss and teeth oscillation iron loss. This aspect is the most significant contributor to stray loss in these devices. The primary source of iron loss is observed in the toothed surfaces and back iron (p_{st}, p_{rt}) of the stator and rotor, particularly when slip frequency is affordable. The Eq. (12) is used to calculate basic loss of stator teeth (P_{st}).

$$p_{st} = k_t p_{ps} {B_p}^{1.7} G_{st} \left(\frac{f_0}{f_r}\right)^{1.3} \tag{12}$$

where p_{ps} is the specific loss in W/kg at 1.0 T, f_0 and f_r are the rated frequency and slip frequency, respectively. k_t represent the responsible for the core loss augmentation caused by mechanical machining (k_t depends on the quality of the material sharpening of cutting tools), The variable B_p represents the magnetic flux factor that arises from the passage of air-gap energy between the stator teeth. The weight of these variables (G_{st}) is able to be determined by employing Eq. (13).

$$G_{st} = \gamma_{ir} N_s b_{bs} L_i k_{fe} (hs + hs_1 + hs_0) \tag{13}$$

where k_{fe} is the winding fill factor. Similarly, the fundamental loss (p_{rt}) of stator back iron (yoke) can be obtained using Eq. (14).

$$p_{rt} = k_r p_{ps} {B_{sb}}^{1.7} G_{rl} \left(\frac{f_0}{f_r}\right)^{1.3} \tag{14}$$

where B_{sb} is the stator back flux density, k_r is the influence of mechanical machining and G_{rl} is the yoke weight, which can be obtained using Eq. (15).

$$G_{rl} = \gamma_{ir} \frac{\pi}{4} L_i k_{fe} \left[{D_{out}}^2 - (D_{out} - 2h_{cs})^2\right] \tag{15}$$

where k_{fe} is the winding fill factor, and h_{cs} is the back iron height. The flux pulsation iron loss is the main component of stray losses and can be calculated using Eq. (16).

$$P_{ir} = 0.5.10^{-4} \left[G_{rl} \left(N_s P_{sr} P_{ss} \frac{f_0}{p_i}\right)^2 + G_{st} \left(N_r P_{fr} P_{fs} \frac{f_0}{p_i}\right)^2\right] \tag{16}$$

where N_r and N_s are the rotor slot number, P_{sr} and P_{fr} are the flux pulsation density losses per kilogram of teeth in the stator and rotor, and P_{ss} and P_{fs} are the tooth flux density pulsation losses in the stator and rotor, respectively. From (12), (14), and (16), the total iron loss that occurs in the spindle motor is calculated by Eq. (17).

$$P_{jt} = (P_{st} + P_{rt}) + P_{ir} \tag{17}$$

3. Design Methodology

The conceptual optimizer was implemented on a fast speeds spindle drive, inspired by an existing industrial device design. The original device featured an estimated power rating of 14 kW, 4 poles, a delta (Δ) connection, it operated during a voltage of 380 V. The spindle device was designed in a circular semi-closed stator slot configuration, as depicted in **Figure 1**. The pertinent characteristics of the device can be found in **Table 1**. Both the stator and rotor metal elements were composed of silicon-iron laminating using a grade of 35h250. Additionally, a copper rotor bar was utilized in the construction of the drive unit.

Table 1. Spindle drive specification

Parameter	Dimension
Inner/outer diameter of Stator (mm)	70/120
Core length (mm)	120
Outer/inner diameter of rotor (mm)	69.3/38
The number of stator/rotor slot	36/32

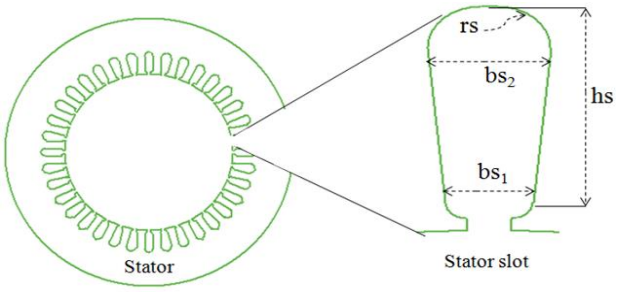

Figure 1. Semi-closed stator slots of the spindle drive

The process of constructing Response Surface Methodology (RSM) models involved using the methods of Design of Experiments (DOE) and Central Composite Design (CCD) techniques. These strategies were used to gather statistical evidence from multiple sources, with the intention of creating situations involving performing exploratory investigations and assessing the effects of various parameters and the corresponding levels. The ultimate objective was to determine the optimal configuration of stator variables. The purpose of the experiments was to obtain the results for various combinations of elements related to the stator connection reactance and iron leaking regions. The mathematical representation of the link between the response and the design variables is a second-order model (18), as mentioned in reference [13].

$$y = \beta_o + \sum_{i=0}^{n} \beta_i x_i + \sum_{i=0}^{n-1} \sum_{j=i+1}^{n} \beta_{ij} x_i x_j + \sum_{i=0}^{n} \beta_{ii} x_i^2 + \varepsilon \tag{18}$$

where y is the power response share, β_0, β_i, β_{ij}, and β_{ii} are the second-order coverage of the matching formula, n is the total of parameters, and x_0.....x_n are the values of the design parameters that have been adjusted according to a specific scaling factor. The quadratic and interaction terms of the model are employed to forecast the ideal value of the stator variables. For this stage, the CCD method was employed, utilizing five distinct experimental variables and five corresponding levels, as outlined in **Table 2**. **Table 3** presents the orthogonal array pertaining to the chosen variable, together with the pertinent experimental data for the investigation of stator leaking reactance and iron loss distribution. The anticipated values of the stator parameters are estimated based on the research findings as expressed in Eq. (19).

$$x = \frac{real\ value\ of\ x - \left(\frac{a}{2}\right)}{\left(\frac{b}{2}\right)} \tag{19}$$

where

$$a = A_U + A_L \tag{20}$$

$$b = A_U - A_L \tag{21}$$

Table 2. Variables and levels in response surface analysis

Factor	Definition	-2	-1	0	1	2
A	h_s (mm)	5.5	6.5	7.5	8.5	9
B	b_{s2} (mm)	4	4.4	4.8	5.2	5.6
C	r_s (mm)	0.5	0.8	1.3	1.6	2
D	Wire diameter (*wd*) (mm)	0.381	0.429	0.511	0.643	0.767
E	Winding turns per slot (coil)	24	36	48	60	72

Table 3. CCD data with 5-factors and 5-levels analysis

No Exp	Actual factor					Iron loss (W)	Stator leakage (Ohm)	Efficiency (%)	Torque (Nm)
	h_s	b_{s2}	r_s	wd	coil				
1	8.5(1)	5.2(1)	1.6(1)	0.429(-1)	36(-1)	366.88	2.31	87.64	11.00
2	6.5(-1)	4.4(-1)	1.6(1)	0.643(1)	60(1)	57.16	6.25	81.39	3.67
3	7.5(0)	4.8(0)	1.3(0)	0.511(0)	48(0)	164.15	4.07	88.34	6.07
4	6.5(-1)	5.2(1)	0.8(-1)	0.643(1)	60(1)	59.10	6.14	81.21	3.71
5	7.5(0)	4.8(0)	1.3(0)	0.767(2)	48(0)	175.76	4.01	92.08	6.62
6	7.5(0)	4.8(0)	1.3(0)	0.381(-2)	48(0)	145.26	4.08	82.34	5.35
7	7.5(0)	4.8(0)	2(2)	0.511(0)	48(0)	169.07	4.05	88.30	6.04
8	6.5(-1)	5.2(1)	1.6(1)	0.429(-1)	60(1)	57.78	6.13	70.68	3.38
9	6.5(-1)	4.4(-1)	0.8(-1)	0.429(-1)	60(1)	52.04	6.22	70.67	3.35
10	8.5(1)	4.4(-1)	1.6(1)	0.643(1)	36(-1)	367.63	2.29	91.23	14.05
11	7.5(0)	4.8(0)	1.3(0)	0.511(0)	24(-2)	755.61	0.88	77.00	33.88
12	7.5(0)	4.8(0)	0.5(-2)	0.511(0)	48(0)	158.78	3.99	88.37	6.10
13	8.5(1)	5.2(1)	1.6(1)	0.643(1)	60(1)	70.73	6.28	81.12	3.65
14	7.5(0)	4.8(0)	1.3(0)	0.511(0)	48(0)	164.15	4.02	88.34	6.07
15	8.5(1)	5.2(1)	0.8(-1)	0.643(1)	36(-1)	375.54	2.22	91.18	14.57
16	7.5(0)	4.8(0)	1.3(0)	0.511(0)	48(0)	164.15	4.02	88.34	6.07
17	6.5(-1)	4.4(-1)	0.8(-1)	0.643(1)	36(-1)	303.08	2.20	91.61	14.66
18	6.5(-1)	4.4(-1)	1.6(1)	0.429(-1)	36(-1)	297.39	2.24	88.09	11.18
19	6.5(-1)	5.2(1)	0.8(-1)	0.429(-1)	36(-1)	305.06	2.17	88.01	11.38
20	8.5(1)	4.4(-1)	0.8(-1)	0.429(-1)	36(-1)	334.84	2.33	87.85	10.93
22	8.5(1)	4.4(-1)	1.6(1)	0.429(-1)	60(1)	62.02	6.50	70.76	3.27
23	7.5(0)	4.8(0)	1.3(0)	0.511(0)	48(0)	164.15	4.02	88.34	6.07
24	8.5(1)	4.4(-1)	0.8(-1)	0.643(1)	60(1)	64.09	6.36	81.21	3.62
25	7.5(0)	5.6(2)	1.3(0)	0.511(0)	48(0)	177.15	3.95	88.29	6.14
26	7.5(0)	4.8(0)	1.3(0)	0.511(0)	72(2)	45.26	9.00	75.83	2.10
27	6.5(-1)	5.2(1)	1.6(1)	0.643(1)	36(-1)	333.56	2.17	91.39	14.85
28	8.5(1)	5.2(1)	0.8(-1)	0.429(-1)	60(1)	64.32	6.31	70.80	3.33
29	7.5(0)	4.8(0)	1.3(0)	0.511(0)	48(0)	164.15	4.02	88.34	6.07
30	7.5(0)	4.8(0)	1.3(0)	0.643(1)	48(0)	171.84	4.01	90.80	6.42
31	7.5(0)	4(-2)	1.3(0)	0.511(0)	48(0)	154.85	4.11	88.35	5.98
32	5.5(-2)	4.8(0)	1.3(0)	0.511(0)	48(0)	140.09	3.91	88.49	6.16

4. Stator and Iron Leakage Analysis using RSM

The present investigation aims to examine the impact of variations in stator characteristics on the spinning part of the motor's torque and efficiency. Specifically, the investigation focuses on the stator and iron leakage reactance, and magnetic flux connection.

4.1. Analysis of Stator and Leakage Reactance by Considering Stator Parameters

Table 3 presents an examination of stator leaks and iron leakage, taking into account the stator parameters and utilizing the CCD results from experiments. This work presents two second-order polynomial Eq. (18) that demonstrate the correlation between the specified parameters h_{s2}, b_{s2}, r_s, wire diameter (wd), and coil. These models showcase the link within these variables.

$$\begin{aligned} Iron\ loss = {} & 169.498 + 13.568h_s + 5.805b_{s_2} + 3.152rs + 6.373wd - 150.727coil \\ & - 5.269h_s^2 - 4.090bs_2^2 - 4.608rs^2 - 5.419wd^2 + 54.519coil^2 \\ & + 0.191hs.bs_2 + 0.117hs.rs + 0.583hs.wd - 10.670hs.coil \\ & + 0.325bs_2.rs - 0.049bs_2.wd - 3.841bs_2.coil - 0.034rs.wd \\ & - 2.425rs.coil - 3.795wd.coil \end{aligned} \quad (22)$$

$$Stator\ leakage = 4.03150 + 0.064h_s - 0.042b_{s2} + 0.014rs - 0.018wd + 2.021coil - 0.001h_s^2 - 0.001bs_2^2 - 0.004rs^2 + 0.003wd^2 + 0.227coil^2 - 0.005hs.bs_2 + 0.006hs.rs - 0.019hs.wd + 0.022hs.coil - 0.007bs_2.rs + 0.006bs_2.wd - 0.017bs_2.coil - 0.005rs.wd + 0.004rs.coil + 0.002wd.coil \quad (23)$$

Figure 2 presents the contour plots depicting the variations in stator leakage and iron losses in relation to the stator parameters. The boost in the values of *hs* and b_{s2}, as depicted in **Figure 2a** leads to an upsurge in the Iron loss. Additionally, a greater number of windings turns per slot and a greater b_{s2} result in larger stator leaking, as illustrated in **Figure 2b**. The reduction in lost iron might be observed in **Figure 2c** due to the utilization of minuscule wire dimensions and hs. To minimize stator leaking, it is necessary to reduce both the amount of winding turns per slot and the dimension of the stator, as seen in **Figure 2b** and **Figure 2d**. Additionally, the h_s parameter has an impact on the stator leaking response, as depicted in **Figure 2d**. The stator leaking and loss of iron can be influenced by increasing the values of the larger h_s and b_{s2} parameters, as well as by adjusting the number of windings turns per slot. The findings from the examination of variance (ANOVA) study indicate the influence of individual stator parameters on both iron losses and stator leaking reactance, as depicted in **Figure 3**. It has been demonstrated that to achieve optimal performance in spindle motors, characterized by minimal losses of iron and stator leaking reactance, the selection of suitable stator characteristics is crucial.

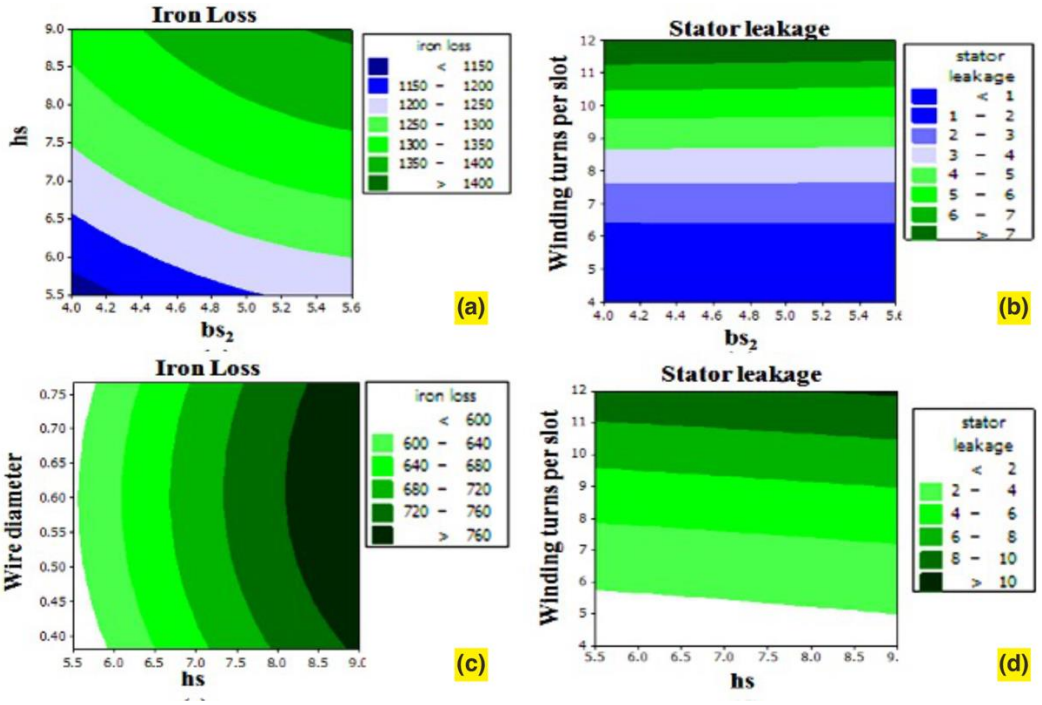

Figure 2. Contour plot simulation with: (a) h_s and b_{s2} with iron loss, (b) winding turn per slot (coil) and b_{s2} with stator leakage, (c) wire diameter and hs with iron loss, (d) winding turn per slot and hs with stator leakage.

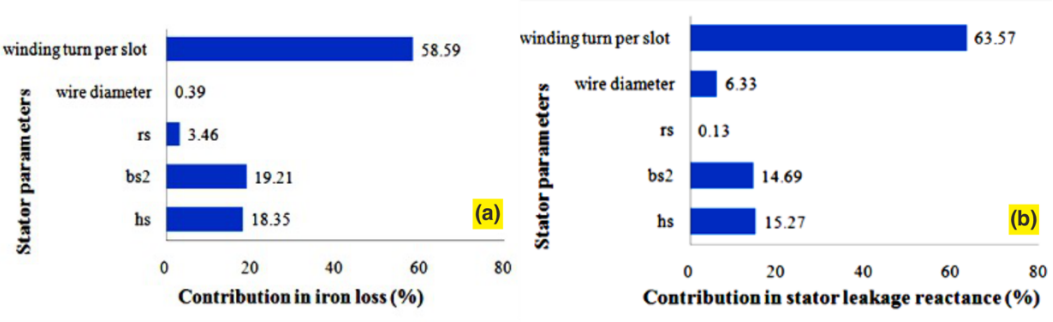

Figure 3. The involvement of every stator variable: (a) iron leakage, (b) stator linking reactance

4.2. Effects of Stator Linking, Magnetic Flux Connection, and Iron Leakage on Spindle Drive Torque and Efficiency

The interconnections between stator leaking, magnetic flux connection, iron losses, torque, and efficiency can be deduced by analyzing the data from experiments shown in **Table 3**, alongside

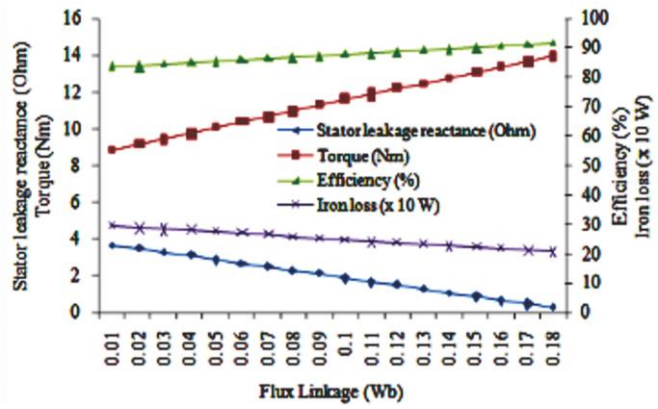

Figure 4. Effect of stator leakage reactance

by utilizing the second order polynomial formulas (22) and (23), while performing a flux connection finite element computation. An upward trend in stator leaking of the spindle motor results in a corresponding increase in iron losses [14]. Hence, it can be shown from **Figure 4** that the magnetic flux linkage and torque of the spindle motor exhibit a drop, while the efficiency remains relatively unaffected. Additionally, this phenomenon results in the division of the magnetic flux line circulation generated by the winding of the stator within the stator slots into various types of leaking, including zigzag leakage, slot leakage, end-turns leakage, as well as magnetizing reactanceand reduced magnetizing energy. In addition, an increase in stator leaking reactance results in a decrease in the flux density of both the stator teeth and the airgap.

4.3. Attaining Optimal Design

The trials were conducted on a prototype spindle drive, and the results obtained from the response surface methodology (RSM) were subsequently optimized. This optimization process involved the utilization of certain objective functions:

$$\text{Amplify } f_1(x) = \text{Efficiency} \tag{24}$$

$$\text{Amplify } f_2(x) = \text{Torque} \tag{25}$$

Subject to

$$x_L \leq x \leq x_U \tag{26}$$

where x is the newly introduced design parameter, and x_L and x_U are the lower and upper bound of the design parameter, respectively. According to the summary from the preceding analysis in (Suction 4.2), increased torque and efficiency result in higher magnetic flux connection and reduced iron leakage. As a result, efficiency and torque are the target functions that determine appropriate stator component architecture, whereas stator leaking reactance, magnetic flux connection, and loss of iron constitute limitations. As illustrated in **Figure 5**, the optimization procedure yields the optimum set of the stator criteria, which have high torque and efficiency. The *hs* is 8 mm, b_{s2} is 4.8 mm, r_s is 1.5 mm, wire diameter is 0.767 mm and coil per phase is 48. Applying these requirements, the spindle motor was manufactured for validation purposes.

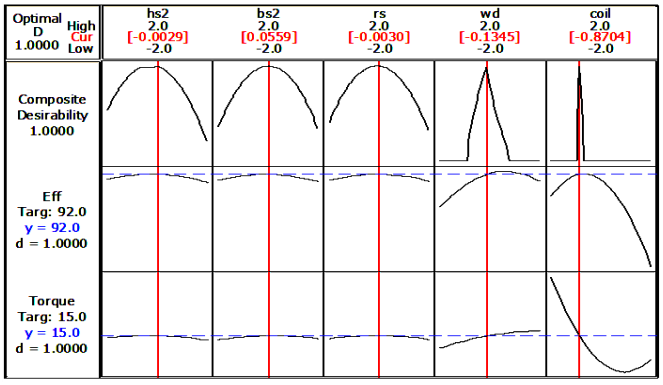

Figure 5. Optimal value of the result of RSM technique

5. Simulation and Experimental Results

Figure 6 depict the steps involved in manufacturing and quality control evaluation, which include no-load testing and machine balance analysis [15]. **Table 4** summarizes the results of the FEM and experimental measurements. It demonstrates that the best model produces higher magnetic flux connection and lower iron losses than the industry design in 3000, 12000, and 21000 rpm assignments. The flux connection FEM study findings demonstrate that the ideal construction creates higher magnetic flux linking in addition to decreased stator loss response (**Figure 7a**). Furthermore, as compared to the industrial design, this design minimizes the current waveform in the stator winding (**Figure 7b**) and converts induced current into an electromagnetic force, resulting in higher torque and efficiency (**Table 4**). Because of the high stator leakage reactance in the

industrial design, high current is induced in the stator winding, resulting in flux pulsation density losses and increased iron loss, as illustrated in **Figure 7c** and **Figure 7d.**

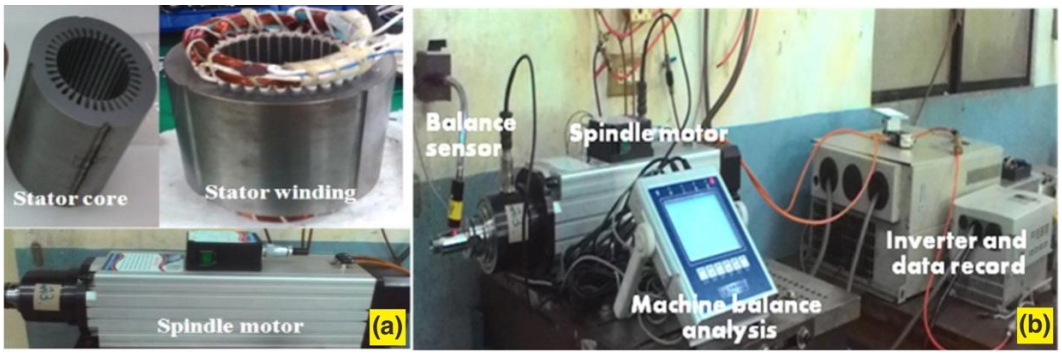

Figure 6. (a) Manufacturing process of the spindle motor, (b) Product quality measurement process

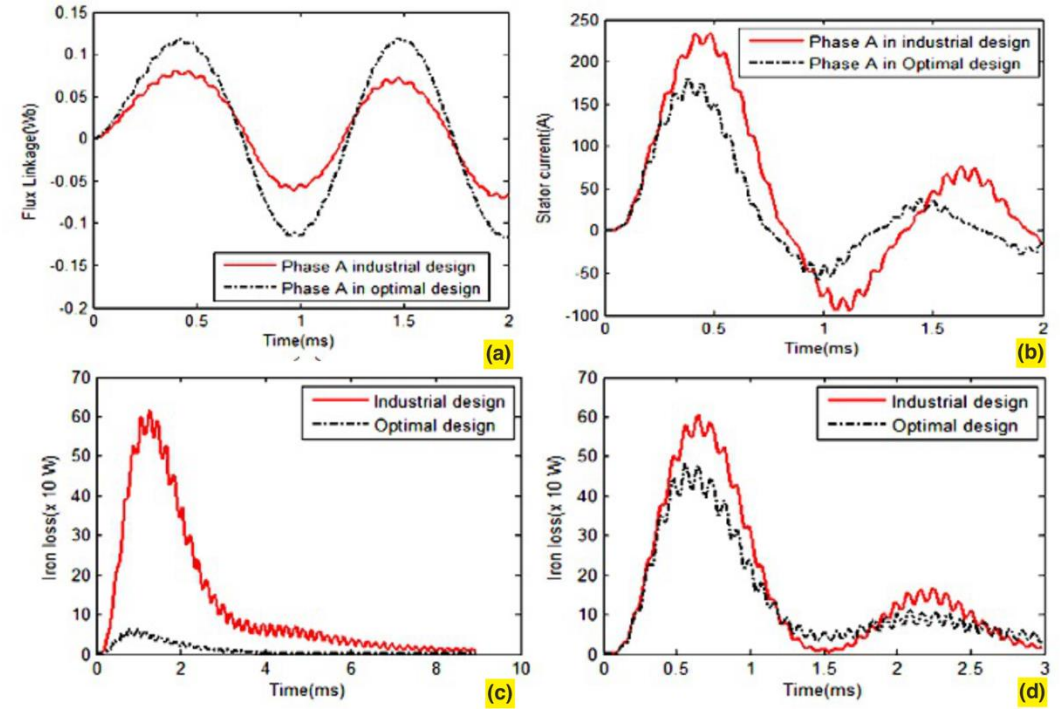

Figure 7. Flux linkage FEM analysis for flux linkage, stator current, and iron loss characteristics: (a) flux linkage distribution in 3000 rpm (b) stator current in 3000 rpm (c) iron loss in 3000 rpm (d) iron loss in 21000 rpm

Table 4. Summary of the simulation and experiment results

Parameter	Experiment and analysis results			
	Industrial design	Optimal design	Experiment results	Error (%)
3000 rpm				
Stator leakage reactance (Ohm)	0.432	0.355	0.345	2.82
Magnetic flux linkage (Wb)	0.154	0.704	0.703	0.14
Iron loss (W)	37.79	34.49	33.49	2.89
Efficiency (%)	53.88	67.38	69.53	3.19
12000 rpm				
Stator leakage reactance (Ohm)	1.686	1.277	1.267	0.78
Magnetic flux linkage (Wb)	0.159	0.166	0.162	2.41
Iron loss (W)	256.54	219.89	215.42	2.03
Efficiency (%)	79.94	88.19	88.57	0.43
21000 rpm				
Stator leakage reactance (Ohm)	2.967	2.351	2.53	7.61
Magnetic flux linkage (Wb)	0.082	0.085	0.084	1.18
Iron loss (W)	319.87	272.96	273.67	0.26
Efficiency (%)	86.45	92.23	92.29	0.07

The results of the 2D Finite Element Method (FEM) transient field analysis demonstrate that the ideal structure exhibits a higher magnetic flux connection, resulting in a more favorable arrangement of magnetic flux in the stator teeth [13]. Specifically, the most effective design yields magnetic flux densities of 1.18 T in the stator teeth, 0.58 T in the air-gap, and 1.87 T in the rotor teeth. In comparison, the industrial design exhibits lower magnetic flux densities of 0.86 T in the

stator teeth, 0.44 T in the airgap, and 1.14 T in the rotor teeth. **Figure 8** illustrates the attributes of magnetic flux dispersion. According to the data shown in **Table 4**, it can be observed that the percentage of error between the simulation and measured findings is below 5% for the rotational speeds of 3000 and 12000 rpm. However, for the rotational speed of 21000 rpm, the percentage of error in the stator leakage reactance is recorded as 7.61%. One potential factor contributing to this error % could be the variation in the applied value of the stator slot geometry. This discrepancy may arise due to the manufacturing process, which allows to produce stator slots with varying coefficients, resulting in increased stator leakage reactance. In general, the measured outcomes exhibit a high level of concurrence with the simulation outcomes. Hence, the enhancement of the stator structure can lead to an increase in magnetic flux linkage, a reduction in iron loss, and an overall improvement in the performance of the spindle motor [3], [16].

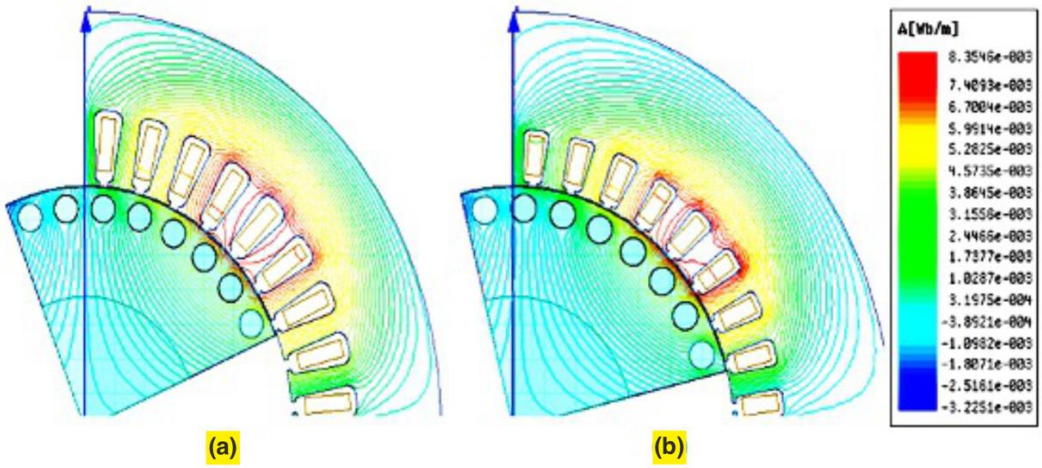

Figure 8. Magnetic flux line distribution in 21000 rpm: (a) Industrial design (b) Optimal design

6. Conclusion

This work effectively demonstrates the successful optimization of stator configurations to enhance performance in magnetic flux connection and minimize iron loss in high-speed spindle drives used in machine tool operations. The Response Surface Methodology (RSM), Design of Experiments (DOE), and Finite Element Method (FEM) collectively offer the most efficient design solution. The stator parameters consist of five components, namely hs, bs2, rs, the wire diameter, and coil per slot, each of which has five levels. The findings were analyzed utilizing the Finite Element Method (FEM) and subsequently verified through experimental validation. The utilization of Finite Element Method (FEM) and Design of Experiments (DOE) in the engineering process results in an ideal design that exhibits enhanced magnetic flux connection and reduced iron leakage compared to the existing industrial design. In industrial design, the presence of high stator leakage reactance leads to the induction of high current in the stator winding, resulting in flux pulsation and density losses. These losses contribute to increased iron loss and a reduction in the torque output of the spindle motor. The accuracy of the suggested model is confirmed through the comparison of the simulated outcomes with the measured findings. In general, the error rate is estimated to be around 7%. The appropriate configuration of the spindle motor is advantageous for its utilization in high-speed spindle motors employed in machine tools operating within the range of 3000 to 21000 rpm.

Acknowledgments

The author would like to thank Rector Universitas Negeri Padang for financial support and the Automotive Department for supporting research facilities.

Authors' Declaration

Authors' contributions and responsibilities - The authors made substantial contributions to the conception and design of the study. The authors took responsibility for data analysis, interpretation, and discussion of results. The authors read and approved the final manuscript.

Funding – Universitas Negeri Padang.

Availability of data and materials - All data are available from the authors.

Competing interests - The authors declare no competing interest.

Additional information – No additional information from the authors.

References

[1] S. Sachin, K. Manickavasagam, and A. T. Sriram, "Effect of core losses on thermal analysis of 3ϕ- Squirrel Cage Induction Motor using lumped parameter thermal model," *Materials Today: Proceedings*, vol. 80, pp. 724–730, Jan. 2023, doi: 10.1016/J.MATPR.2022.11.076.

[2] O. Payza, Y. Demir, and M. Aydin, "Investigation of losses for a concentrated winding high-speed permanent magnet-assisted synchronous reluctance motor for washing machine application," *IEEE Transactions on Magnetics*, vol. 54, no. 11, Nov. 2018, doi: 10.1109/TMAG.2018.2848881.

[3] K. Kawanishi, K. Matsuo, T. Mizuno, K. Yamada, T. Okitsu, and K. Matsuse, "Development and Performance of High-Speed SPM Synchronous Machine," *2018 International Power Electronics Conference, IPEC-Niigata - ECCE Asia 2018*, pp. 169–176, Oct. 2018, doi: 10.23919/IPEC.2018.8507781.

[4] K. Bataineh and A. Al Rabee, "Design Optimization of Energy Efficient Residential Buildings in Mediterranean Region," *Journal of Sustainable Development of Energy, Water and Environment Systems*, vol. 10, no. 2, Jun. 2022, doi: 10.13044/J.SDEWES.D9.0385.

[5] M. Srbinovska and M. Cundeva-Blajer, "Optimization Methods for Energy Consumption Estimation in Wireless Sensor Networks," *[Journal of Sustainable Development of Energy, Water and Environment Systems]*, vol. [7], no. [2], p. [261]-[274], Jun. 2019, doi: 10.13044/J.SDEWES.D6.0244.

[6] W. Purwanto, H. Maksum, T. Sugiarto, M. Nasir, and F. Rizal, "The Effect of Stator Winding Parameter Design to The Magnetic Flux Characteristics in High-Speed Motor Applications," *Journal of Theoretical and Applied Information Technology*, vol. 30, no. 12, 2019.

[7] W. Purwanto, H. Maksum, T. Sugiarto, Risfendra, A. Baharudin, and Marno, "Optimal design of stator slot geometry for high-speed spindle induction motor applications," *2019 International Conference on Information and Communications Technology, ICOIACT 2019*, pp. 811–816, Jul. 2019, doi: 10.1109/ICOIACT46704.2019.8938493.

[8] M. Aishwarya and R. M. Brisilla, "Design of Energy-Efficient Induction motor using ANSYS software," *Results in Engineering*, vol. 16, p. 100616, Dec. 2022, doi: 10.1016/J.RINENG.2022.100616.

[9] S. Chakrabarty and R. Kanagaraj, "Design, Simulation, and Analysis of Switched Reluctance Motor for High-Speed Applications," *2021 National Power Electronics Conference, NPEC 2021*, 2021, doi: 10.1109/NPEC52100.2021.9672508.

[10] N. Rossi *et al.*, "Design and thermal assessment of a high performance electric motor for racing applications," *Proceedings - 2021 IEEE Workshop on Electrical Machines Design, Control and Diagnosis, WEMDCD 2021*, pp. 52–57, Apr. 2021, doi: 10.1109/WEMDCD51469.2021.9425681.

[11] F. Xu *et al.*, "Comparison of 2-pole Slotted High-speed Motors with Toroidal and Tooth-coil Windings," *Proceedings of 2022 IEEE 5th International Electrical and Energy Conference, CIEEC 2022*, pp. 3410–3415, 2022, doi: 10.1109/CIEEC54735.2022.9845996.

[12] W. Purwanto, T. Sugiarto, H. Maksum, D. S. Putra, and E. Alwi, "Comparison of Three Topologies Rotor to Improve Efficiency and Torque for High-Speed Spindle Motor Applications," *Proceedings of ICAITI 2018 - 1st International Conference on Applied Information Technology and Innovation: Toward A New Paradigm for the Design of Assistive Technology in Smart Home Care*, pp. 176–181, Jul. 2018, doi: 10.1109/ICAITI.2018.8686718.

[13] M. Appadurai, E. Fantin Irudaya Raj, and K. Venkadeshwaran, "Finite element design and thermal analysis of an induction motor used for a hydraulic pumping system," *Materials Today: Proceedings*, vol. 45, pp. 7100–7106, Jan. 2021, doi: 10.1016/J.MATPR.2021.01.944.

[14] J. Li *et al.*, "Research on the Effect of Spindle Speed on the Softening and Hardening Characteristics of the Axial Operating Stiffness of Machine Tool Spindle," *Lubricants 2022, Vol. 10, Page 132*, vol. 10, no. 7, p. 132, Jun. 2022, doi: 10.3390/LUBRICANTS10070132.

[15] L. A. Pereira, M. Perin, L. F. A. Pereira, J. R. Ruthes, F. L. M. de Sousa, and E. C. P. de Oliveira, "Performance estimation of three-phase induction motors from no-load startup test without speed acquisition," *ISA Transactions*, vol. 96, pp. 376–389, Jan. 2020, doi:

10.1016/J.ISATRA.2019.05.028.

[16] F. Xu *et al.*, "Influence of Slot Number on Electromagnetic Performance of 2-pole High-Speed Permanent Magnet Motors with Toroidal Windings," *2020 15th International Conference on Ecological Vehicles and Renewable Energies, EVER 2020*, Sep. 2020, doi: 10.1109/EVER48776.2020.9242986.